

Generative Adversarial Network in Medical Imaging: A Review

Xin Yi, Ekta Walia, Paul Babyn

Abstract—Generative adversarial networks have gained a lot of attention in general computer vision community due to their capability of data generation without explicitly modelling the probability density function and robustness to overfitting. The adversarial loss brought by the discriminator provides a clever way of incorporating unlabeled samples into the training and imposing higher order consistency that is proven to be useful in many cases, such as in domain adaptation, data augmentation, and image-to-image translation. These nice properties have attracted researcher in the medical imaging community and we have seen quick adoptions in many traditional tasks and some novel applications. This trend will continue to grow based on our observation therefore we conducted a review of the recent advances in medical imaging using the adversarial training scheme in the hope of benefiting researchers that are interested in this technique.

Index Terms—Deep learning, Generative adversarial network, Generative model, Medical Imaging, Review

I. INTRODUCTION

WITH the resurgence of deep learning in general computer vision starting from 2012 [76], the adoption of deep learning methods in medical imaging has increased dramatically during the past few years. It is estimated that there are over 400 papers published in 2016 and 2017 in major medical imaging related conference venues and journals [85]. The wide adoption of deep learning in the medical imaging community is due to its demonstrated potential to complement image interpretation, augment image representation and classification. Near or super human performance has been achieved in many tasks including skin cancer diagnosis [37], detection of diabetic retinopathy [48] and organ segmentation in adult chest X-rays [29].

In this article, we focus on one of the most interesting and recent breakthroughs in the field of deep learning- Generative Adversarial Networks (GANs) and their prospective applications in the field of medical imaging.

GANs are a special type of neural network model where two networks are trained simultaneously, with one focused on image generation and the other centered on discrimination. It provides a way to learn deep representations without extensively annotated training data. It has gained attention in industry and academia due to its robustness to overfitting, and capabilities to capture data distributions making image generation tasks more straightforward. This model has achieved

state-of-the-art performance in many image generation tasks, including text-to-image synthesis [153], super-resolution [81], and image-to-image translation [175].

Unlike deep learning which has its roots traced back to 1980s [42], the concept of adversarial training is relatively new. Although there are many challenges still need to be solved, such as training stability, generated image quality and diversity, there has been significant progress since 2014 with its adoption into medical imaging field. In this paper, we provide a general overview of GANs, and describe their potential applications in medical imaging. We also attempt to identify the challenges that need to be solved to enable further successful application in the field of medical imaging.

In order to get a comprehensive review of all relevant works on GANs in medical imaging, we searched databases like PubMed, arXiv, international conference proceedings of Medical Image Computing and Computer Assisted Intervention (MICCAI), SPIE Medical Imaging, IEEE International Symposium on Biomedical Imaging (ISBI), and international conference on Medical Imaging with Deep Learning (MIDL). We also incorporated cross referenced works not included in the above searching process. Since there are research publications coming out every month, without losing generality, we set the cut off time of the search as July 30, 2018. Works on arXiv that only report preliminary results are excluded from this review. A general statistics of these papers based on task, imaging modality and year can be found in Figure 1.

The rest of the paper is structured as followed. We begin with a introduction to GANs and its research directions in Section II. It is followed by a comprehensive review of the publications in medical image analysis using GANs in Section III including but not limited to the field of radiology, histopathology, and dermatology. We categorize all the works according to canonical tasks: reconstruction, image synthesis, segmentation, classification, detection, registration, and others. Section IV discusses prospective applications and identifies open challenges.

II. BACKGROUND

A. Vanilla GAN

The vanilla GAN [45] is one type of generative model where we can directly draw samples from the desired data distribution without the need to explicitly model the underlying probability density function. It consists of two neural networks: generator G and discriminator D . The input to G , z is pure random noise sampled from a prior distribution $p(z)$, which is commonly chosen to be a Gaussian or an uniform distribution for

Both X. Yi and P. Babyn are with the Department of Medical Imaging, University of Saskatchewan, Saskatoon, SK, S7N 0W8 Canada

E. Walia works with Philips Canada and also holds adjunct position with the Department of Medical Imaging, University of Saskatchewan, Saskatoon, SK, S7N 0W8 Canada

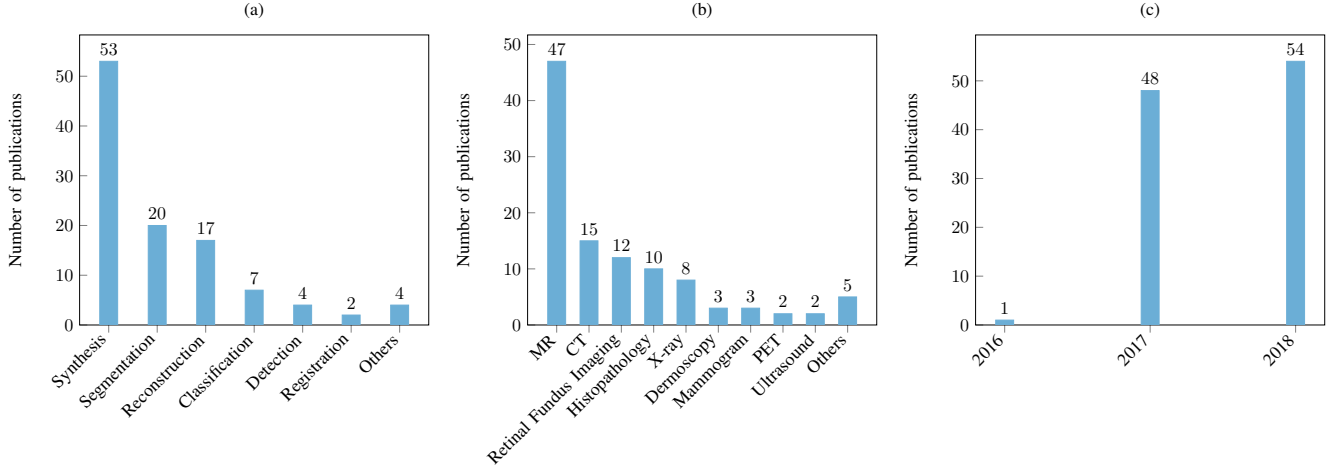


Fig. 1: (a) Categorization of GAN related papers according to canonical tasks. (b) Categorization of GAN related papers according to imaging modality. (c) Number of GAN related papers published in total each year. Note that some works performed various tasks and conducted evaluation on datasets with different modalities. We counted these works multiple times in plotting these graphs. For works that are on cross domain image transfer, we counted based on the source domain.

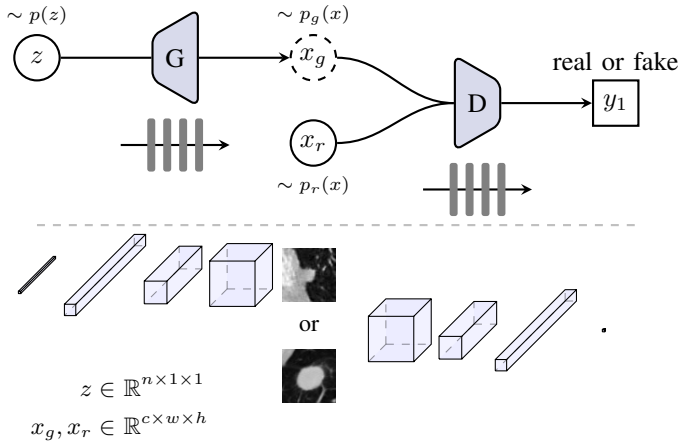


Fig. 2: Schematic view of the vanilla GAN for lung nodule synthesis. Top of the figure shows the the network configuration. The part below shows the input, output and the internal feature representations of the corresponding networks: generator G and discriminator D.

simplicity. The output of G, x_g is expected to have visual similarity with the real sample x_r that is drawn from the real data distribution $p_r(x)$. We denote the non-linear mapping function learned by G parametrized by θ_g as $x_g = G(z; \theta_g)$. The input to D is either the real or generated samples. The output of D, y_1 is a single value indicating the probability of the input being real or fake sample. The mapping learned by D parametrized by θ_d is denoted as $y_1 = D(x; \theta_d)$. The generated samples form a distribution $p_g(x)$ which is desired to be an approximation of $p_r(x)$ after successful training. Top of Figure 2 shows an illustration of the configuration of vanilla GAN. G in this example is generating 2D slice of CT lung nodules.

D's objective is to differentiate these two groups of images whereas G is trained to confuse D as much as possible.

Intuitively, the generator network G could be viewed a forger trying to produce some counterfeit material, and the discriminator network D could be regarded as a police man trying to detect the forged items. In an alternative view, we can perceive the generator as receiving a reward signal from the discriminator depending upon whether the generated data is accurate or not. The gradient information is back propagated from the discriminator back to the generator network, so the generator adapts its parameters in order to produce an output image that can fool the discriminator network. The training objectives of G and D can be expressed mathematically as:

$$\begin{aligned} \mathcal{L}_D^{GAN} &= \max_D \mathbb{E}_{x_r \sim p_r(x)} [\log D(x_r)] \\ &\quad + \mathbb{E}_{x_g \sim p_g(x)} [\log(1 - D(x_g))], \\ \mathcal{L}_G^{GAN} &= \min_G \mathbb{E}_{x_g \sim p_g(x)} [\log(1 - D(x_g))], \end{aligned} \quad (1)$$

As can be seen that D is simply a binary classifier with maximum log likelihood objective. If the discriminator D is trained to optimality before the next generator G updates, then minimizing \mathcal{L}_G^{GAN} is proven to be equivalent to minimizing the Jensen–Shannon (JS) divergence between $p_r(x)$ and $p_g(x)$ [45]. The desired outcome after the training is that samples formed by x_g approximates the real data distribution $p_r(x)$.

B. Variants of GAN

The GAN loss formulation is regarded as saddle point optimization problem [155] and the training of the GAN is often accomplished by gradient-based methods. G and D are trained alternatively so that they evolve together. However, there is no guarantee of balance between the training of G and D with the JS divergence. As a consequence, one network may inevitably be more powerful than the other, which in most cases, is D. When D becomes too strong as opposed to G, the generated samples become too easy to be separated from

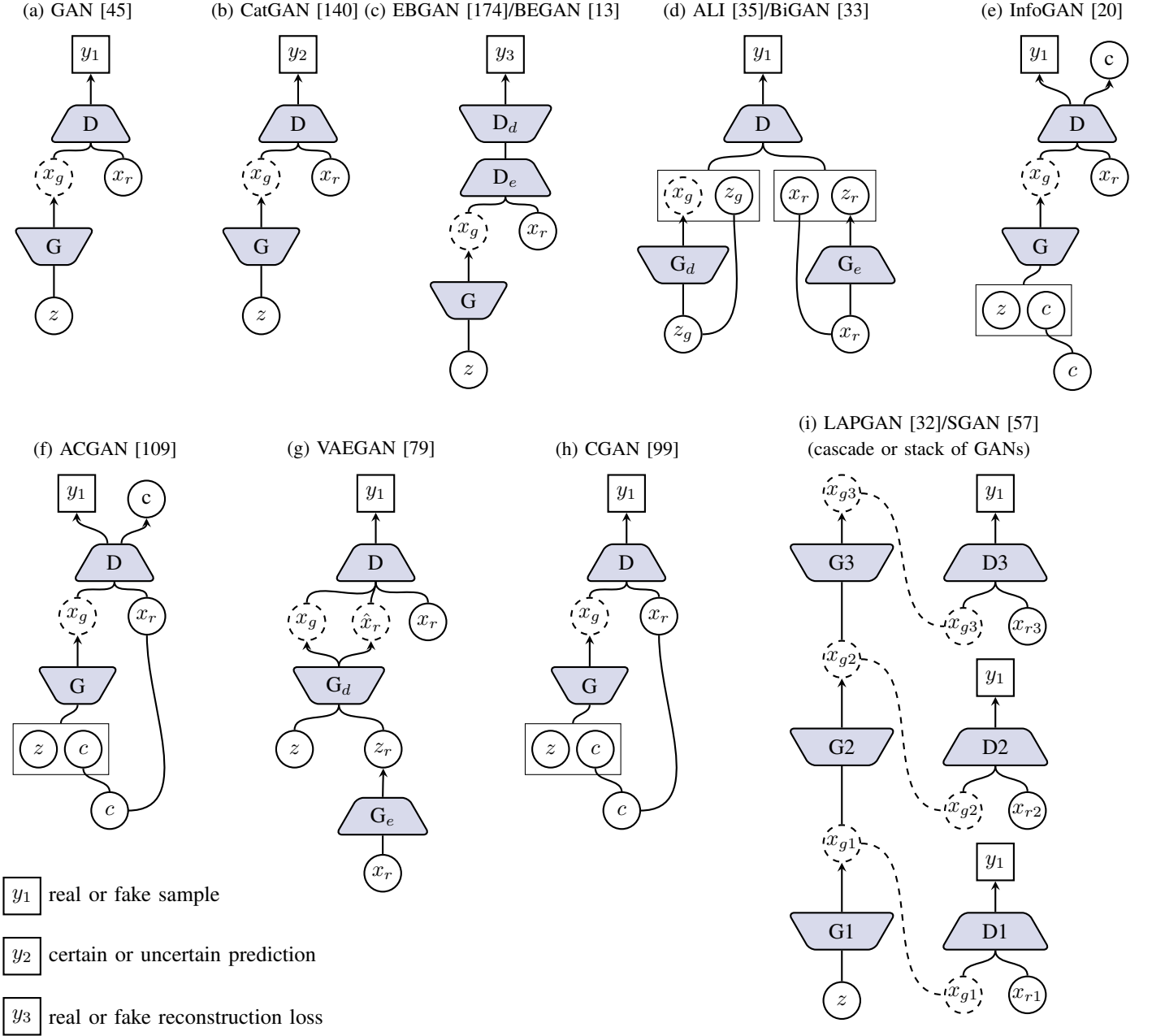


Fig. 3: A schematic view of variants of GAN. c represents the conditional vector. In CGAN and ACGAN, it is the discrete categorical code (e.g. one hot vector) that encodes class labels and in InfoGAN it can also be continuous code that encodes attributes. x_g generally refers the generated image but can also be internal representations as in SGAN.

real ones, therefore only vanishing gradients can be provided for further training of G . This happens more frequently when generating high resolution images due to the difficulty of generating meaningful high frequency details.

Another problem commonly faced in training of GANs is mode collapse, which as the name indicates, is a case when the learned distribution $p_g(x)$ by G focuses on a few limited modes of the data distribution $p_r(x)$. Hence instead of producing diverse images, it always generates a limited set of samples.

1) **Varying objective of D :** In order to stabilize the training and also to avoid mode collapse, different losses for D have

been proposed, such as f-divergence (f-GAN) [108], least-square (LSGAN) [95], hinge loss [100], and Wasserstein distance (WGAN, WGAN-GP) [3, 47]. Among them, Wasserstein distance is arguably the most popular metric. In order for Wasserstein distance to work, $D(x; \theta_d)$ must be locally Lipschitz (gradient with respect to θ_d is bounded). As an alternative to the real/fake discrimination scheme, Springenberg proposed an entropy based objective where real data is encouraged to make confident class predictions [140]. Generated data on the other hand is forced to output even numbers across all interested classes. This work was referred as categorical generative adversarial network (CatGAN, Figure 3 b). In

CycleGAN so that images can be translated between two sets of unpaired samples (Figure 4 b) [175]. Note that at roughly the same time Kim et al. came up with essentially the same idea and named their method DiscoGAN [71]. We chose CycleGAN to represent this idea in the rest of this paper for the sake of simplicity. Another technique named UNIT (Figure 5) can also perform unpaired image-to-image transform by combining two VAEs together with each one responsible for one modality but sharing the same latent space [86]. For G conditioned on images, task related loss is used for the generator. For example, if it is for image restoration, then it is usually reconstruction loss that is either in the form of pixel-wise loss between the restored image and the groundtruth or cycle consistency loss. For segmentation, the commonly used losses are Dice loss [98] and pixel-wise cross entropy loss. These image-to-image translation frameworks are very popular in medical imaging community due to their general applicability.

Beyond that, the conditional input can also be text descriptions [167], object locations [119, 120], surrounding image context [113], and sketches [128].

3) **Varying architecture**: Fully connected layer was used as the building block in vanilla GAN but was later on replaced by fully convolutional downsampling/upsampling layers in DCGAN [117] as this was shown to have better training stability hence quickly populated the literature. As shown in Figure 2, the generator in DCGAN architecture works on random input noise vector by successive upsampling operations eventually generating an image from it. Two important ingredients of this architecture is the use of BatchNorm [60] to regulate the extracted feature scale and LeakyRelu [89] to prevent dead gradients. Very recently, Miyato et al proposed a spectral normalization layer that normalized the weights in the discriminator to regulate the scale of feature response values [100]. It exhibited good performance and could potentially replace other regularization techniques, such as gradient penalty regularization [47], Dragan regularization [72]. With the training stability improved, some works have also incorporated residual connections into both the generator and discriminator and experimented with much deeper networks [47, 100]. Another interesting work is also from Miyato et al where the authors proposed a projection based way to incorporate the conditional information instead of direct concatenation [101].

Directly generating large size images is hard, therefore some works proposed tackling it in a progressive manner. In LAPGAN [32], Denton et al. proposed a stack of GANs, each of which adds higher frequency details into the generated image. In SGAN, a cascade of GANs is also used but each GAN is used to generate increasingly lower level representation [57]. These representations are compared with the hierarchical representations extracted from a discriminatively trained model during the training. This progressive idea was also explored in conditional setting [144]. Karras et al. adopted an alternative way where they progressively growing the generator and discriminator by adding new layers to them rather than stacking another GAN on top of the preceding one [69].

Schematic illustrations of the reviewed commonly used

GAN-based methods are shown in Figure 3. They are GAN, CatGAN, EBGAN/BEGAN, ALI/BiGAN, InfoGAN, AC-GAN, VAEGAN, CGAN, LAPGAN, SGAN. Three popular image-to-image translation cGAN based frameworks (pix2pix, CycleGAN, and UNIT) are shown in Figure 4 and 5. For a more in-depth review and empirical evaluation of these different variants of GAN, we refer the reader to [56, 27, 77] for more information.

III. APPLICATIONS IN MEDICAL IMAGING

There are two ways of viewing GANs. The first is focusing on the generative model G, which helps explore and discover the underlying structure of the training data and learns to generate new images from it. This property makes GANs very promising in the medical imaging domain to cope with issues related to data scarcity and patient privacy. Another way is focusing on the discriminator D, which can be regarded as a learned prior for the normal images so that it can be used as regularizer or detector. You can see all the existing GAN related works in medical imaging can be more or less fit into these two groups. Figure 6 gives some examples on GAN related applications.

A. Reconstruction

This is essentially a image to image translation problem where the conditioned inputs of all the cGANs are compromised in certain forms, such as low spatial resolution, noise contamination, under-sampling, or aliasing.

1) **CT denoising**: Computed tomography (CT) denoising is of particular interest because of the cancer related concern regarding ionizing radiation. Traditional deep learning methods minimize the pixel-wise loss between the denoised image and ground truth, which inevitably casts a blur effect on the resultant denoised image caused by averaging over all plausible solutions. The adversarial loss can be directly borrowed to reduce the blur effect by driving the output image to stay on the manifold of natural sharp image. Several pioneer works have already tried it.

Wolterink et al. used cGAN for cardiac CT image denoising [152]. They have shown that CT denoising is possible without the routine dose counterparts in the training by sacrificing certain amount of small structural details. Yi et al. performed low dose CT denoising with both adversarial loss and a sharpness loss expecting to explicitly constrain the sharpness of the denoised CT especially for the low contrast regions [160]. They conducted thorough experiments with images covering various anatomic regions and a series of dose levels. Yang et al. used cGAN by optimizing the Wasserstein distance between the low dose CT distribution and the high dose CT distribution for abdominal CT image denoising [159]. A perceptual loss adopted from natural images is used to ensure perceptual similarity between the denoised and ground truth high dose CT. Kang et al. used CycleGAN to denoise multiphase coronary CT angiography [68]. Although the low dose CT and routine dose CT images are unpaired, they are both from the same cardiac volume. The authors argue that the learning thus is more effective than learning from totally

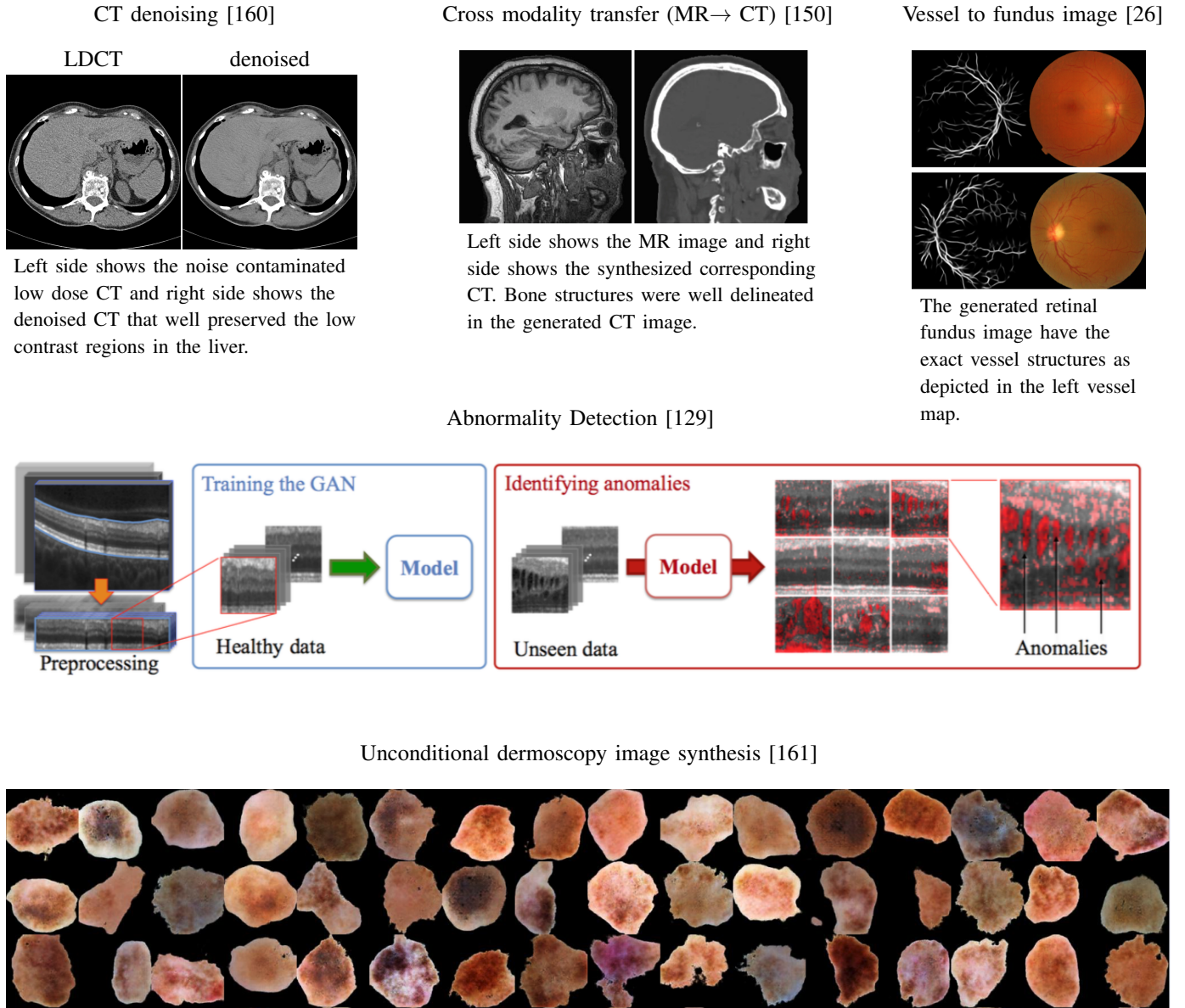


Fig. 6: Example applications using GANs. Figures are directly cropped from the corresponding papers.

different images. You et al. replaced the perceptual loss used in [159] with a structure similarity loss and extend the input of the generator from 2D to 3D patch [162]. They argue that the perceptual loss computed from a network trained on natural images may cause anatomical distortions in the reconstruction.

2) **MR image Reconstruction:** The application of GAN in magnetic resonance (MR) image reconstruction has mostly been used to accelerate the image acquisition process. Acquisition of high spatial resolution MR image scan can be time consuming and can cause patient anxiety and increased risk of motion artifacts. Reducing the acquisition time and raw data needed is especially useful in time-sensitive applications, such as fetal, cardiac, and lung imaging. The idea is similar to in CT denoising, which is partially sampling the acquired data and then using cGAN to estimate the missing data.

Shitrit et al. used cGAN for accelerating MR image re-

construction [135]. The generator produces missing k-space samples by conditioning on undersampled k-space data while the discriminator differentiates the reconstructed MR image from the real MR image (both are obtained by inverse Fourier transform of the k-space signal). Quan et al. employed a reconstruct and refine scheme by using adversarial loss together with a cyclic consistency loss for MR image reconstruction from undersampled k-space data [115]. The cyclic consistency is enforced in a form that the reconstructed MR image from aliased image should be close to the groundtruth image reconstructed from fully sampled data, and if we applied the sample mask and Fourier transform to the reconstructed MR image, the result should be close to the acquired raw k-space data. Mardani et al. did similar job for MR image reconstruction but only ensure image space consistency [96]. In [164], Yu et al. used a generator to directly estimate the reconstructed MR

image based on the under-sampled reconstruction. They further incorporated perceptual loss computed from a pretrained VGG-net [137] into the optimization framework to ensure perceptual similarity. Sánchez et al. performed reconstruction on 3D volumetric MR images with adversarial loss and gradient loss [127]. Chen et al. also performed 3D reconstruction on undersampled MR images but use a densely connected network to reduce memory consumption and Wasserstein loss for the discriminator to stabilize the training [22]. Kim et al. [70] and Dar et al. [31] found that if incorporating high resolution image acquired with a different MR sequence in the input, the generated image quality can be further improved.

3) **PET denoising**: Positron emission tomography (PET) is commonly used in clinical oncology to evaluate cancer metastasis. Instead of using an external X-ray tube as in CT, a radioactive tracer is injected to the body for the image acquisition. The general public is also concerned about health related issues regarding to the ionizing radiation and efforts are needed to lower the radiation exposure while not compromising the diagnostic quality.

Wang et al. used a cascade formulation of cGAN to progressively refine the reconstructed image [145]. Each generator in the cGAN sequences processes 3D inputs as similar to [152] but with a modified network architecture. Armanious et al. proposed a general framework named MedGAN that is able to perform PET denoising [4]. It is essentially a variant of pix2pix with modified generator structures and additional losses, i.e. perceptual loss, style-content loss.

4) **Superresolution (SR)**: Mahapatra et al. used adversarial loss in creating high resolution retinal fundus images from corresponding low resolution images [92]. A saliency loss is also proposed by reweighting each pixel's importance based on its perceptual relevance. The super-resolved image is shown to behave closely to the original high resolution image in the vessel segmentation task. Ravì et al. performed super-resolution on endomicroscopy images which usually has few informative pixels due to hardware constraints [118]. They introduced a physical acquisition based loss using a unpair training scheme to regulate the generated image structure.

The reconstruction works were summarized in Table I.

B. Medical Image Synthesis

Medical image synthesis is one of the most important use of GAN due to the privacy issues related to medical image data and the general insufficient number of positive training samples. Lack of experts annotating medical images poses another challenge for the adoption of supervised training methods. Additionally, patient consent is required if diagnostic images are intended to be used in a publication or released in public domain [110]. Although there are some ongoing collaborative efforts in multiple healthcare agencies aiming to build large number of open access datasets, e.g. Biobank, national biomedical imaging archive (NBIA), and the cancer imaging archive (TCIA), this issue remains to be solved and constrains the number of images researchers might have access to.

Traditional ways to expand training sample include scaling, rotation, flipping, translation, elastic deformation [136]. But

these transformations do not account for variations resulted from difference imaging protocol, sequence, not to mention lesion variations such as size, shape, location and appearance. GANs provide a more generic solution and have been used in numerous works for synthesizing training images with promising results.

1) **Unconditional Synthesis**: Calimeri et al. used LAPGAN for brain MR image synthesis [16]. Similar work was done in [49] but with WGAN. Chuquicuma et al. simulated lung nodules and conducted visual Turing test for evaluation of the generated samples [24]. Lafarge et al. [6] used GAN to synthesize skin lesion images. Wolterink et al. used WGAN to synthesize blood vessels by parametrizing vessel geometries as 1D signals based on the central vessel axis [151]. Chest X-ray images were synthesized using DCGAN by Madani et al. [90]. They used two GANs to generate normal and abnormal (cardiomegaly) chest X-rays and evaluated the image quality in both classification as well as radiologist grading task. Bermudez et al. used DCGAN to generate 2D brain MR scans [12]. Even neuroradiologist admitted comparable quality of the generated images as to real ones, they noted that anatomic accuracy has been overlooked in the current generation process. The unconditional synthesis works were summarized in Table III.

2) **Cross modality synthesis**: This is also a image to image translation problem where images from one modality is transformed to the other, e.g. MR to CT, or translating across different acquisitions within a modality, e.g. T1 MR to T2 MR. As will be seen that most of the methods reviewed in this section share a lot of similarities to those in section III-A. The translation is deemed to be useful for multiple reasons, one of which is to reduce the acquisition time and cost. Another reason is to generate new training samples with the appearance being constrained by the anatomical structures delineated in the available modality.

MR to CT synthesis is deemed useful in MR-only radiotherapy treatment planning. An accurately synthesized CT could avoid excessive exposure of radiation and provide electron densities of the body tissues in predicting the dose distribution during the therapy. Nie et al. performed MR to CT transformation with 3D cGAN and adopted auto-context model (ACM) to refine the generated CT [105, 106]. The ACM they adopted was essentially a cascade of cGANs trained in a sequence with the input conditioned on the generated output of the last cGAN. This proposed method was also used to generate 7T MR image from 3T MR image in [106] (7T MR image provides higher spatial resolution and contrast than 3T but is also more expensive and practically infeasible to obtain). Emami et al. used cGAN to directly generate CT from T1 MR in 2D plane [36].

In [14], PET images were generated based on the corresponding CT and annotation maps of manually drawn high uptake regions. Their experiments have also shown that a tumour detection network trained on the synthetic PET images performs very close to a same network trained on real PET images. Cohen et al. demonstrated a similar concept for synthesizing PET images from CT [10]. Their virtual PET was found to be beneficial in reducing false positives in live

Modalities	Publications	Aligned data	Method	Losses	Dataset
CT	[152] (3D)	✗	pix2pix*	L_{adv}	–
	[160]	✓	pix2pix*	$L_{adv}, L_{image}, L_{sharp}$	Piglet
	[159]	✓	pix2pix*	$L_{adv}, L_{image}, L_{percep.}$	2016 LDCT Grand Challenge
	[68]	✗	CycleGAN*	$L_{adv}, L_{cycle}, L_{identity}$	–
	[162]	✓	pix2pix*	$L_{adv}, L_{image}, L_{structure}$	2016 LDCT Grand Challenge
MR	[116]	✓	pix2pix*	$L_{adv}, L_{image}, L_{freq}$	IXI, Data Science Bowl, knee
	[96]	✓	pix2pix*	L_{adv}, L_{image}	–
	[164]	✓	pix2pix*	$L_{adv}, L_{image}, L_{percep.}$	IXI, MICCAI 2013 Grand Challenge
	[127] (3D)	✓	pix2pix*	$L_{adv}, L_{image}, L_{grad.}$	ADNI
	[22] (3D)	✓	cGAN	L_{adv}, L_{image}	–
	[70]	✓	pix2pix*	L_{adv}, L_{image}	BRATS 2015
	[31]	✓	pix2pix*	L_{adv}, L_{image}	BRATS 2015, IXI, MIDAS
	[135]	✓	pix2pix*	L_{adv}, L_{image}	–
	[145] (3D)	✓	cascade cGAN	L_{adv}, L_{image}	–
	[4]	✓	pix2pix*	$L_{adv}, L_{image}, L_{percep.}, L_{style-content}$	–
PET	[92] (SR)	✓	pix2pix*	$L_{adv}, L_{image}, L_{percep.}, L_{saliency}$	–
Endomicroscopy	[118] (SR)	✗	pix2pix*	$L_{adv}, L_{physical}, L_{reg}$	–

TABLE I: List of publications on medical image reconstruction. Note that * following the method denotes some modifications on the basic framework either on the generator architecture or on the employed losses. A brief description of the losses can be found in Table II.

Losses	Requirement	Remarks
L_{adv}	–	Adversarial loss introduced by the discriminator. It can take the form of cross entropy loss, hinge loss, least square loss etc. as discussed in Section II-B1.
L_{image}	Aligned training pair	Element-wise loss in image domain to ensure structure similarity to the target when aligned training pair is provided.
L_{cycle}	–	Element-wise loss to ensure self-similarity during cycled transformation when unaligned training pair is provided.
L_{grad}	Aligned training pair	Element-wise loss in the gradient domain to emphasize edges.
L_{edge}	Aligned training pair	Similar to L_{grad} but using gradient feature map as a weight to image pixels.
L_{sharp}	Aligned training pair	Element-wise loss in a feature domain computed from a pre-trained network, which is expected to be the image sharpness with focus on low contrast regions.
L_{shape}, L_{seg}	Annotated pixel-wise label	Loss introduced by a segmentor to ensure faithful reconstruction of anatomic regions
L_{percep}	Aligned training pair	Element-wise loss in a feature domain computed from a pre-trained network which expected to conform to visual perception.
$L_{structure}$	Aligned training pair	Patch-wise loss in the image domain computed with SSIM which is claim to better conform to human visual system.
$L_{style-content}$	Aligned training pair	Style and content loss to ensure similarity of image style and content. Style is defined as the Gram matrix which is basically the correlation of low-level features.
$L_{self-reg}$	–	Element-wise loss for self regulation. Suitable for cases where the generated image and the input have a lot in common.
L_{steer}	Aligned training pair	Element-wise loss in a feature domain which is computed from steerable filters with focus on vessel-like structures.
$L_{classify}$	Aligned image-wise label	Loss introduced by a classifier to get semantic information
L_{freq}	Aligned training pair	Element-wise loss in frequency domain (k-space) used in MR image reconstruction.
L_{kl}	–	Kullback–Leibler divergence which is commonly seen in variational inference to ensure the approximation close to the posterior distribution.
$L_{saliency}$	Aligned training pair	Element-wise loss in a feature domain which is expected to be the saliency map.
$L_{physical}$	Physical model	Loss introduced by a physical image acquisition model.
L_{reg}	–	Application dependent loss to further regulate generated image.

TABLE II: A brief summary of different losses used in the reviewed publications. The requirement column specifies conditions to be fulfilled in order to use the corresponding loss.

Imaging modalities	Publications	Method	Dataset	Quantitative measure
MR	[16] (brain)	LAPGAN	–	kernel density, inception score, human observer
	[49] (brain)	WGAN	BRATS 2016	human observer
	[8] (brain)	PGGAN	BRATS 2017	visualize latent vector
	[8] (brain)	DCGAN	BLAS	human observer
CT	[24] (lung nodule)	DCGAN	LIDC-IDRI	human observer
X-ray	[90] (chest)	DCGAN	NIH PLCO	classification (data augmentation)
Mammography	[75]	PGGAN	–	–
Retinal fundus imaging	[8]	PGGAN	–	visualize latent vector
	[78]	DCGAN	DRIVE	classification
Dermoscopy	[6]	LAPGAN	ISIC2017	JS divergence/Wasserstein distance between normalized color histogram
	[161]	CatGAN+ WGAN	ISIC2016, PH2	classification (data augmentation)

TABLE III: List of publications on unconditional medical image synthesis.

Modalities	Pulications	Aligned Data	Method	Losses	Dataset	Quantitative measure
MR → CT	[105, 106] (brain, pelvic)	✓	Cascade GAN	$L_{adv}, L_{image}, L_{grad}$	ADNI	MAE, PSNR
	[36] (brain)	✓	cGAN	L_{adv}, L_{image}	–	MAE, SSIM, PSNR
	[34] (cardiac, feature space)	✗	domain adapt	L_{adv}	–	segmentation
CT → MR	[65] (brain)	✗	CycleGAN	$L_{adv}, L_{cycle}, L_{image}$	–	MSE, MAE, PSNR
	[18] (cardiac)	✗	CycleGAN	L_{adv}, L_{cycle}	Link	segmentation
	[172] (cardiac 3D)	✗	CycleGAN*	$L_{adv}, L_{cycle}, L_{shape}$	–	segmentation
MR ↔ CT	[58] (spleen)	✗	CycleGAN*	$L_{adv}, L_{cycle}, L_{seg}$	–	segmentation
	[18] (cardiac)	✗	CycleGAN	L_{adv}, L_{cycle}	–	segmentation
	[51] (musculature and skeleton)	✗	CycleGAN*	$L_{adv}, L_{cycle}, L_{grad}$	–	mutual information, segmentation
CT → PET	[150] (brain)	✗	CycleGAN	L_{adv}, L_{cycle}	–	MAE, PSNR
	[14] (thorax)	✓	cGAN	L_{adv}, L_{image}	–	MAE, PSNR
	[10] (liver)	✓	FCN+cGAN	L_{adv}, L_{image}	–	MAE, PSNR, lesion detection
PET → CT	[4] (brain)	✓	cGAN*	$L_{adv}, L_{image}, L_{percep.}, L_{style-content}$	–	MSE, PSNR, SIIM, VIF, UQI, LPIPS
MR → PET	[148] (brain)	✓	cascade cGAN	L_{adv}, L_{image}	–	task specific statistics
PET → MR	[23] (brain)	✓	pix2pix	L_{adv}, L_{image}	ADNI	SSIM, task specific statistics
Synthetic → Real	[52] (histopathology)	✓	synthesizer+cGAN	$L_{adv}, L_{image}, L_{seg}$	MICCAI 15, 17 challenges	segmentation, human
Real → Synthetic	[94] (endocscopy)	✗	cGAN	$L_{adv}, L_{self-reg}$	–	depth estimation
	[170] (X-ray)	✗	CycleGAN*	$L_{adv}, L_{cycle}, L_{seg}$	–	segmentation
	[19] (X-ray)	✗	CycleGAN*	$L_{adv}, L_{cycle}, L_{seg}$	Montgomery, JSRT	segmentation
T1 → T2 MR	[30] (brain)	✗	CycleGAN	L_{adv}, L_{cycle}	MIDAS, IXI, BRATS2015	PSNR, SSIM
	[158] (brain)	✗	cGAN	L_{adv}, L_{image}	BRATS2015	MAE, PSNR, MI, cross modality registration, segmentation
	[149] (brain)	✗	CycleGAN, UNIT	$L_{adv}, L_{image}, L_{cycle}$	Human Connectome	MAE, PSNR, MI
T1 → FLAIR MR	[163] (brain, 3D)	✓	cGAN	L_{adv}, L_{image}	BRATS 2015	PSNR, NMSE, segmentation
T1, T2 → MRA	[111] (brain)	✓	pix2pix*	$L_{adv}, L_{image}, L_{steer}$	IXI	PSNR, segmentation
3T → 7T MR	[106] (brain)	✓	Cascade GAN	$L_{adv}, L_{image}, L_{grad}$	–	MAE, PSNR
Histopathology	[11]	✗	cGAN+classifier	$L_{adv}, L_{edge}, L_{classify}$	MITOS-ATYPIA, GlaS, OCHD	classification
	[166]	✗	InfoGAN	$L_{adv}, L_{image}, L_{recon}, L_{kl}$	–	NMI
	[131]	✗	CycleGAN	$L_{adv}, L_{image}, L_{cycle}$	MITOS-ATYPIA, Camelyon16	SSIM, PSNR, FSIM, classification
Hyperspectral hist. → H&E	[7] (lung)	✓	cGAN	L_{adv}, L_{image}	Link	MSE, SSIM

¹ SSIM: structural similarity [147] ² PSNR: peak signal to noise ratio ³ MAE: mean absolute error ⁴ MSE: mean square error
⁵ VIF: visual information fidelity [133] ⁶ UQI: universal quality index [146] ⁷ LIPIPS: learned perceptual image patch similarity [169]
⁸ NMI: normalized median intensity

TABLE IV: List of publications on cross modality image synthesis.

Modalities	Conditional information	Publications	Method	Dataset	Quantitative measure
Ultrasound	Probe location	[54] (fetus)	cGAN	–	human observer
Retinal fundus imaging	Vessel map	[173]	cGAN	DRIVE, STARE, HRF	segmentation
	Vessel map	[46]	dual cGAN	DRIVE	segmentation, KL divergence
	Vessel map	[25]	segmentor+pix2pix	DRIVE	Q_v score, ISC
	Vessel map	[26]	adversarial VAE+cGAN	DRIVE, Messidor	ISC
	Vessel map, Lesion map	[2]	cGAN	DRiDB, DIARETDB1, Messidor	Q_v score, Haemorrhage detection
MR	Segmentation map	[103]	coarse-to-fine boundary-aware	BRATS 2015	segmentation
Histopatholog	Segmentation map	[130]	pix2pix	–	human observer
X-ray	Different view, segmentation map	[44]	pix2pix/CycleGAN	–	–

¹ Q_v : [74] ² ISC: Image Structure Clustering [107]

TABLE V: List of publications on other conditional image synthesis.

lesion detection. The method they proposed consists of a full convolutional network (FCN) [88] which generates initial results that are subsequently refined by a cGAN.

Different MR acquisition sequences provide different tissue contrast. Dar et al. used the cycle loss for transformation between T1 and T2 weighted MR images [30]. Yang et al.'s work is similar to [30], where transformations were across T1, T2 and T2-Flair MR images [158]. They further evaluated their method in cross-modality registration and segmentation task with improved results. Olut et al. generated MR Angiography (MRA) conditioned on both T1- and T2- weighted MR images [111]. They proposed a vessel sensitive loss based on steerable filters to improve faithful generation of vessel structures. Yu et al. explored 3D volumes transform from T1-weighted MR to FLAIR image [163]. The output of cGAN was used in a locally adaptive fusion by predicting the final synthesized image as linear combination of the training data. They have demonstrated the quality of the synthesized image by showing an improved segmentation performance of brain tumour when using both the T1 and synthesized FLAIR image. More recently, Armanious et al. proposed a method named MedGAN for the purpose of general image to image translation [4]. They utilized a cascade U-Net as the generator for progressively refining the generated image, and incorporated perceptual loss, style-content loss into the cGAN framework. Perceptual study conducted by radiologists demonstrated the effectiveness on three different tasks including PET to CT translation, MR motion correction, and PET denoising. MR to PET synthesis was conducted in [148] for myelin content measurement with a cascade cGAN (two in total) operating on 3D volumes. They have shown that the generator in the first cGAN can delineate a general anatomy and physiology structures and the second cGAN building on top can refine and fill in the missing tissue myelin content. Choi et al. directly used pix2pix framework to transform PET to MR and have shown the generated MR is accurate for amyloid quantification [23].

The above works all require co-registered training data and relied on L_1 or L_2 distance in the image space to ensure data fidelity. The registration is possible for brain or bone structures but is very challenging for moving objects such as heart. Therefore, Chatsias et al. proposed to use CycleGAN for cardiac synthesis [18] between MR and CT volumes. The quality of the synthesized images were manifested in a downstream cardiac CT segmentation task with a performance boost. Huo et al. extends Chatsias et al.'s work by merging the segmentation network into the synthesis workflow which enables end-to-end training [58]. They have shown that splenomegaly segmentation in CT is possible without any groundtruth annotation of CT volumes. Wolterink et al. adopted the same methodology for brain CT image synthesis from MR image [150]. They have found that training using unpaired images were even better than using aligned images, which was most likely resulted from the fact that rigid registration could not handle very well local alignment in the throat, mouth, vertebrae, and nasal cavities. In [51] Hiasa et al. further incorporated gradient consistency loss in the training to improve the accuracy at the boundaries.

Zhang et al. have found that just using cycle loss in the cross modality synthesis is not enough to mitigate geometric distortions in the transformation [172]. Therefore, they employed a shape consistency loss that is obtained from two segmentors (segmentation network). Each segmentor segments the corresponding image modality into semantic labels and provides implicit shape constraints on the anatomy during the translation. To make the whole system end-to-end trainable, semantic labels of training images from both modalities are required. Zhang et al. proposed to also use segmentor in the cycle transfer [170]. But their setting only has labels in one modality. Therefore, the segmentor is trained offline and fixed during the training of the image transfer network. The exact same idea was explored by Chen et al. for domain adaption of chest X-rays from different sources [19]. Jin et al. performed CT to MR synthesis for patients in the aging society where metal implants such as cardiac pacemakers and artificial joints can be a problem in MR [65]. They trained their model with both paired and unpaired samples and have shown that it achieved better results than just using one kind of data alone. Welander et al. did a comparison of CycleGAN and UNIT in the task of transforming between T1 and T2 MR images [149]. They found both performing almost equally well.

Mahmood et al.'s work performed a reverse synthesis, where they proposed to use cGAN to transform real endoscopy image to a synthetic-like representation by removing patient specific textures, such as vascular pattern [94]. They demonstrated the effectiveness through the task of monocular depth estimation for endoscopy images where the depth estimation network was trained on synthetic images.

Beyond radiology, conditional image to image synthesis has also gained a lot of interest in histopathology. Bayramoglu et al. used cGAN for virtual H&E Staining of hyper-spectral lung histology images [7]. Hou et al. adopted a synthesis and refine approach to generate histopathology images. cGAN was used in this case to give synthetic images a realistic look [52]. They evaluated their proposed model with a nucleus segmentation task and demonstrated on-par or even better performance than pure supervised methods. Another popular adoption of cGAN in histopathology is for stain normalization. Hematoxylin and Eosin (H&E) staining is commonly used to distinguish different tissue components in biopsy. However, the stained tissue exhibits various appearances due to factors such as the inconstancy of staining protocols, and inherent nature of imaging devices. Color normalization is found to be beneficial for a computer assisted diagnosis (CAD) system. Zanjani et al. used a modified version of InfoGAN for the transformation [166, 165], where the latent attribute information is part of the color system matrix. Shaban et al. proposed to use CycleGAN to cope with this problem [131]. BenTaieb et al. used adversarial loss together with a task specific loss introduced from a classification network to ensure that there is no class specific information loss in the color normalization process [11].

The cross modality synthesis works were summarized in Table IV.

3) **Other synthesis:** Here we review papers that generate images based on segmentation maps, text, locations or syn-

thetic images etc.

Hu et al. proposed the use of cGAN to generate anatomically accurate ultrasound images based on spatial position of the freehand probe [54]. Zhao et al. simulated retinal fundus images and neuronal images with cGAN by conditioning on segmentation maps [173]. They have further shown that using synthetic images together with real images can boost the segmentation performance. Guibas et al. proposed to first use GAN to generate vessel structures and subsequently use them in a cGAN framework to generate photo realistic retinal fundus images [46]. Similar work was performed in [25] where Costa et al. also adopts a two stage generation process for retinal fundus images. The difference lies in that the conditional vessel structures were obtained by applying a pre-trained segmentation network on unlabeled retinal images in [25]. Later on, Costa et al. reformulated their generation setting by using a variational autoencoder for synthesizing vessel structures [26]. Beyond generating normal retinal images from vessel masks, Pujitha et al generated abnormal retina images with haemorrhages by conditioning the generator on both the vessel and lesion masks [2]. The quality of the synthetic image was evaluated in a haemorrhage detection system. It was shown that by using synthetic data together with the original annotated training data, the detection system got a roughly 25% boost on the sensitivity.

Mok et al. used cGAN to augment training images for brain tumour segmentation [103]. The generator was conditioned on segmentation map and generated brain MR image in a coarse to fine manner. To ensure the tumour got well delineated with clear boundary in the generated image, they further made the generation multitasking by forcing the generator to output the tumour boundaries in the generation process. Galbusera et al. used the pix2pix framework to synthesize sagittal X-rays of the lumbar spine based on an annotated segmentation map [44]. In the same work, they also performed X-ray view transfer, i.e. from sagittal to coronal and vice versa. Senaras et al. used pix2pix to generate Ki67-stained whole slide images (patch) based on segmentation map [130].

C. Segmentation

Generally, researchers are using pixel or voxel-wise loss such as cross entropy for segmentation. Despite the fact that U-net [123] was used to combine both the low-level and high-level features, there is no guarantee of spatial consistency in the final segmentation map. Traditionally, conditional random field (CRF) and graph cut methods are usually adopted for segmentation refinement by incorporating spatial correlation. The limitation is that they only take into account pair-wise potentials and therefore might cause serious boundary leakage in low contrast regions. Adversarial losses as introduced by the discriminator on the other hand can take into account high order potentials [157]. In this case, the discriminator can be regarded as a shape regulator. This regulation effect can be also applied to the internal features of the segmentor to achieve domain invariance. *Works discussed in this section use adversarial loss to directly regulate the segmentor instead of using segmentor to regulate the anatomic structure of the*

generated image in the generator as has been done in works shown in Section III-B .

Xue et al. proposed a SegAN network where they adopted adversarial loss for brain tumour segmentation on MR images [154]. They used a multi-scale L_1 loss in the discriminator where features coming from different depth are compared. This was proven to be effective in enforcing the multi-scale spatial constraints of the segmentation maps and the system achieves state-of-the-art performance on BRATS 13 and 15 challenge. Similar work on brain tumour segmentation was performed by Rezaei et al. [121] and Li et al. [83]. The difference is that in [121] and [83], the generator takes heterogenous MR scans of various contrast as provided by BRATS 17 challenge. Moeskops et al. also evaluated the effectiveness of adversarial loss in the task of brain MRI segmentation on MRBrainS13 [102]. Kohl et al. used adversarial loss in the segmentation of prostate cancer on MR images with improved sensitivity [73]. Son et al. also incorporated adversarial loss in retinal image segmentation [139]. They experimentally compared the effect of depth of discriminator on the segmentation performance and found that the deep architecture for discriminating whole images performs the best and has less false positives with fine vessels. Yang et al. evaluated the effect of adversarial loss in the task of liver segmentation from 3D CT volumes [157]. Their generator is essentially a U-net with deep supervisions. Zhang et al. proposed to use both annotated and unannotated images in the segmentation pipeline [171]. The annotated images are used in the same way as in [154, 139, 157] where both element-wise loss and adversarial loss are applied. The unannotated images on the other hand are only used to compute a segmentation map to confuse the discriminator. The effectiveness of the usage of unannotated images is evaluated on both gland and fungus segmentation. Dai et al. applied adversarial loss on lung and heart segmentation in chest X-ray. By evaluation on JSRT and Montgomery dataset, they have demonstrated that the adversarial loss is able to correct the shape inconsistency faced by other methods without adversarial training [29]. Wang et al. performed adversarial training for basal membrane segmentation in histopathology images [143]. Rezaei et al. employed a cascade of cGANs in segmenting myocardium and blood pool in MR images [122]. Izadi et al. applied adversarial loss on skin lesion segmentation [62]. Experiments on DermoFit demonstrated that the adversarial training helps to refine the boundary precision. Shankaranarayana et al. used cGAN for jointly segmenting optic disc and cup for glaucoma screening [132]. Huo et al. used global convolutional network (GCN) [114] as the generator in the pix2pix framework [59]. They have shown the benefits of large receptive field as introduced by GCN and adversarial loss in segmenting abnormally enlarged spleen on MR images. Li et al. combined pix2pix with ACGAN for the segmentation of fluorescent microscopy images of different cell types [82]. They found that the introduction of the auxiliary classifier branch provides regulation to both the discriminator and the segmentor.

Unlike these aforementioned segmentation works where adversarial training is used to ensure higher order structure consistency on the final segmentation maps, Zhu et al.'s

adversarial training scheme is to enforce network invariance to small perturbations of the training samples in order to reduce overfitting on small size dataset [177, 176]. They performed mass segmentation on mammograms and achieved state-of-the-art performance. Kamnitsas et al. used adversarial loss to regulate the learned representation so that the feature representation is domain (different scanners, imaging protocols) invariant [67]. Likewise, Dou et al. also conducted domain adaptation in the feature domain [34] for cardiac segmentation. The adversarial loss is to ensure that the feature distribution of images from both domains (MR and CT) are indistinguishable.

D. Detection

Schlegl et al. used GAN to learn a manifold of normal anatomical variability and proposed a novel anomaly scoring scheme based on the fitness of the latent code of the test image to the learnt manifold [129]. The whole learning process was conducted in an unsupervised fashion and the effectiveness was demonstrated by state-of-the-art performance of anomaly detection on optical coherence tomography (OCT) images. Alex et al. used GAN for brain lesion detection from MR images [1]. The generator was used to model the distribution of normal patches and the trained discriminator was used to compute a posterior probability of patches centered on every pixel in the test image. Chen et al. used an adversarial auto-encoder to learn the data distribution of health brain MR images [21]. The lesion image was then mapped to a image without lesion by exploring the learnt latent space and the lesion could be highlighted by computing the residual of these two images.

All these methods performed abnormality detection in an unsupervised fashion.

E. Classification

Methods reviewed in this section used GANs to generate new training samples as those works in section III-B but solely for the purpose of image-level classification. It provides an alternative way of evaluating the quality of generated samples.

Adar et al. used DCGAN and ACGAN to generate synthetic samples for 3 liver lesion class (cysts, metastases, hemangiomas), and these generated samples are found to be beneficial to the lesion classification task with both improved sensitivity and specificity [41]. Salehinejad et al. performed similar experiment but on chest-Xrays [125]. They used 5 different GANs to generate 5 different classes of chest disease (Pneumothorax, Pulmonary edema, Pleural effusion, Normal, Cardiomegaly) and found that augmenting the real imbalanced datasets with synthesized images achieves better classification performance than just using real imbalanced datasets. Zhang et al.'s work is on incomplete left ventricle coverage detection on cardiac MR images [168]. They used two generators to generate base and apex slice separately and all the synthetic and real images are sent to a single discriminator which outputs both a distribution over image data source and class labels.

Hu et al. [53] used combined WGAN and InfoGAN for unsupervised cell-level feature representation learning in

histopathology images whereas Yi et al. [161] combined WGAN and CatGAN for unsupervised and semi-supervised feature representation learning for dermoscopy images. Both works extract features from the discriminator and built a classifier on top.

Madani et al. [91] adopted the semi-supervised training scheme of DCGAN and used it for chest abnormality classification [91]. In this specific problem, they found that the semi-supervised DCGAN can achieve comparable performance with a traditional supervised CNN with an order of magnitude less labeled data. A similar observation was made by Lahiri et al. in semi-supervised classification of retinal vessel patches [78]. Furthermore, in [91] the authors have also shown that the adversarial loss can reduce domain overfitting by simply supplying unlabeled test domain images as similar to [67].

F. Registration

cGAN can also be used for multi-modal image registration. The generator in this case will be producing transformation parameters, e.g. 6 for 3D rigid transformation and 12 for 3D affine transformation. Then the discriminator discriminates aligned image pairs from unaligned image pairs. A spatial transformation network [63] is usually plugged in between these two networks to enable end-to-end training. Yan et al. performed prostate MR to transrectal ultrasound (TRUS) image registration using this framework [156]. The paired training data was obtained through manual registration by experts.

G. Others

Hu et al. used cGAN to model patient specific motion distribution based on a single preoperative image [55]. They demonstrated the effectiveness in a prostate cancer intervention application. Baumgartner et al. used cGAN for visual attribution, where the generator is used to produce an effect map that highlights regions most accountable for the interested disease [5]. By experimenting on neuro-MR images, they have shown that their proposed method can capture most category specific effects. Mahapatra et al. used CycleGAN for multimodal and unimodal dynamic registration [93]. With experiments on retinal and cardiac images, they have shown that adversarial loss is effective in handling small local transformations. Colorization task was found to be an effective way to explore self-supervision in pretraining of a network [80]. Ross et al. used cGAN to perform re-colorization of endoscopic video data [124] and then finetuned the trained generator for medical instrument segmentation. Their method was used for domain adaptation and found to require only 75% labeled target domain images without sacrificing performance.

IV. DISCUSSION

All the reviewed papers are listed in Table VI based on the corresponding imaging modality. You can also find the complete list of reviewed papers on our GitHub repository¹.

Imaging modalities	Publications
CT	[157], [152], [24], [159], [14], [9], [151], [10], [68], [65], [41], [160], [162], [141], [34]
MR	[135], [18], [73], [58], [102], [16], [83], [115], [121], [164], [96], [150], [1], [55], [105], [84], [154], [168], [67], [5], [163], [39], [156], [127], [116], [51], [93], [49], [36], [111], [8], [30], [148], [4], [106], [158], [172], [21], [122], [22], [149], [141], [70], [103], [12], [59], [31]
PET	[4], [23]
Histopathology	[143], [171], [7], [52], [53], [11], [166], [165], [131], [130]
Mammography	[177], [176], [75]
X-Ray	[125], [104], [29], [90], [91], [44], [170], [19]
Dermoscopy	[142], [62], [161]
Differential interference contrast (DIC) microscopy	[112]
Fluorescence microscopy	[82]
Ultrasound	[54], [156]
Endomicroscopy	[118], [124]
Retinal fundus imaging	[26], [132], [92], [139], [173], [46], [25], [93], [8], [2], [138], [78]
Optical coherence tomography	[129]

TABLE VI: List of publications based on imaging modalities. Note that some works performed various tasks and conducted evaluation on datasets with different modalities. We counted these works multiple times in plotting these graphs. For works that are on cross domain image transfer, we counted based on the source domain.

A. Other interesting applications

Similar to other deep learning neural network models, various applications of GANs demonstrated in this paper have direct bearing on improving radiology workflows and thus patient lives. The strength of GANs however lies in their ability to learn in unsupervised and/or weakly-supervised fashion. In particular, we perceive that image to image translation achieved by cGANs can have various other useful applications in medical imaging. For example, restoration of MR images acquired with certain artifacts such as motion, especially in pediatric setting, helping reduce the number of repeated exams in a radiology center; detection of implanted devices, e.g. staples, wires, tubes, pacemaker and artificial valves on X-rays.

Different imaging modalities work by exploiting tissue response to a certain physical media, such as x-ray, magnetic field and thus can provide supplementary diagnostic information to each other. As a common practice in supervised deep learning, we label a set of images in a certain imaging modality and train a specific network to accomplish a desired task. This process is repeated when switching from one modality to another even if the underlying anatomical structure is the same. A lot of human effort is wasted. Adversarial training, or more specifically unpaired cross modality translation enables reuse of the labels in all modalities.

Exploring GANs for image captioning task [28, 134, 97, 38] can lead to automatic generation of medical imaging reports [66] potentially reducing image reporting times. Success of adversarial text classification [87] also prompts potential utility of GANs in improving the performance of the systems for automatic MR protocol generation from free-text clinical indications [64]. Such automated systems can have direct implications in improvement of MRI wait times which have

been on the rise [40] as well as patient care. cGANs, specifically CycleGAN applications, such as makeup removal [17] can be extended to medical imaging with applications in improving bone x-ray images by removal of artifacts such as casts to facilitate enhanced viewing and helping assess the progress of bone healing efficiently. The success of GANs in unsupervised anomaly detection [129] can help achieve the task of detecting abnormalities in medical images of various modalities, in an unsupervised manner. Such an algorithm can be used for prioritizing radiologist work list, thus optimizing critical findings report turnaround time [43].

Finally, we expect to witness the utility of GANs in medical image synthesis from text descriptions [15], especially for the rare cases, so as to fill in the gap of training samples required for training supervised neural networks for medical image classification tasks.

B. Issues to be solved

In image reconstruction and cross modality image synthesis, most works still adopted traditional shallow reference metrics such as MAE, PSNR, SSIM for quantitative evaluation. But these measures have already found to not corresponding to the visual quality of the image. Even though direct optimization of pixel-wise loss produces a suboptimal (blurry) result, it always gives higher numbers for these measures than using adversarial loss. It becomes increasingly difficult to interpret these numbers in horizontal comparison of GAN-based works especially when extra losses as shown in Table II are incorporated. One way to alleviate this problem is to use down stream tasks such as segmentation or classification to validate the quality of the generated sample. Another way is to recruit domain experts but this approach is expensive, time consuming and hard to scale. Recently, Zhang et al. proposed a perceptual quality metric named learned perceptual image path similarity

¹<https://github.com/xinario/awesome-gan-for-medical-imaging>

(LPIPS) [169] which outperforms previous metrics. It has been adopted in MedGAN [4] for evaluation of the generated image quality but it would be interesting to see its effectiveness for different kinds of medical images as compared to subjective measure from experienced human observer in a more extensive study.

For natural image, the unconditional generated sample quality and diversity is usually measured by inception score [126], the mean MS-SSIM metric among randomly chosen synthetic sample pairs [109], or Fréchet Inception distance (FID) [50]. The validity of these metrics for medical images remain to be explored.

REFERENCES

- [1] V. Alex, M. S. KP, S. S. Chennamsetty, and G. Krishnamurthi. Generative adversarial networks for brain lesion detection. In *SPIE Medical Imaging*, pages 101330G–101330G. International Society for Optics and Photonics, 2017.
- [2] P. Appan and J. Sivaswamy. Retinal image synthesis for cad development. In *International Conference Image Analysis and Recognition*, pages 613–621. Springer, 2018.
- [3] M. Arjovsky, S. Chintala, and L. Bottou. Wasserstein gan. *arXiv preprint arXiv:1701.07875*, 2017.
- [4] K. Armanious, C. Yang, M. Fischer, T. Küstner, K. Nikolaou, S. Gatidis, and B. Yang. Medgan: Medical image translation using gans. *arXiv preprint arXiv:1806.06397*, 2018.
- [5] C. F. Baumgartner, L. M. Koch, K. C. Tezcan, J. X. Ang, and E. Konukoglu. Visual feature attribution using wasserstein gans. *arXiv preprint arXiv:1711.08998*, 2017.
- [6] C. Baur, S. Albarqouni, and N. Navab. Melanogans: High resolution skin lesion synthesis with gans. *arXiv preprint arXiv:1804.04338*, 2018.
- [7] N. Bayramoglu, M. Kaakinen, L. Eklund, and J. Heikkilä. Towards virtual h&e staining of hyperspectral lung histology images using conditional generative adversarial networks. In *Proceedings of the IEEE Conference on Computer Vision and Pattern Recognition*, pages 64–71, 2017.
- [8] A. Beers, J. Brown, K. Chang, J. P. Campbell, S. Ostmo, M. F. Chiang, and J. Kalpathy-Cramer. High-resolution medical image synthesis using progressively grown generative adversarial networks. *arXiv preprint arXiv:1805.03144*, 2018.
- [9] A. Ben-Cohen, E. Klang, S. P. Raskin, M. M. Amitai, and H. Greenspan. Virtual pet images from ct data using deep convolutional networks: Initial results. In *International Workshop on Simulation and Synthesis in Medical Imaging*, pages 49–57. Springer, 2017.
- [10] A. Ben-Cohen, E. Klang, S. P. Raskin, S. Soffer, S. Ben-Haim, E. Konen, M. M. Amitai, and H. Greenspan. Cross-modality synthesis from ct to pet using fcnet and gan networks for improved automated lesion detection. *arXiv preprint arXiv:1802.07846*, 2018.
- [11] A. Bentaieb and G. Hamarneh. Adversarial stain transfer for histopathology image analysis. *IEEE transactions on medical imaging*, 37(3):792–802, 2018.
- [12] C. Bermudez, A. J. Plassard, L. T. Davis, A. T. Newton, S. M. Resnick, and B. A. Landman. Learning implicit brain mri manifolds with deep learning. In *Medical Imaging 2018: Image Processing*, volume 10574, page 105741L. International Society for Optics and Photonics, 2018.
- [13] D. Berthelot, T. Schumm, and L. Metz. Began: boundary equilibrium generative adversarial networks. *arXiv preprint arXiv:1703.10717*, 2017.
- [14] L. Bi, J. Kim, A. Kumar, D. Feng, and M. Fulham. Synthesis of positron emission tomography (pet) images via multi-channel generative adversarial networks (gans). In *Molecular Imaging, Reconstruction and Analysis of Moving Body Organs, and Stroke Imaging and Treatment*, pages 43–51. Springer, 2017.
- [15] C. Bodnar. Text to image synthesis using generative adversarial networks. *arXiv preprint arXiv:1805.00676*, 2018.
- [16] F. Calimeri, A. Marzullo, C. Stamile, and G. Terracina. Biomedical data augmentation using generative adversarial neural networks. In *International Conference on Artificial Neural Networks*, pages 626–634. Springer, 2017.
- [17] H. Chang, J. Lu, F. Yu, and A. Finkelstein. Paired-cycleGAN: Asymmetric style transfer for applying and removing makeup. In *2018 IEEE Conference on Computer Vision and Pattern Recognition (CVPR)*, 2018.
- [18] A. Chartsias, T. Joyce, R. Dharmakumar, and S. A. Tsafaris. Adversarial image synthesis for unpaired multi-modal cardiac data. In *International Workshop on Simulation and Synthesis in Medical Imaging*, pages 3–13. Springer, 2017.
- [19] C. Chen, Q. Dou, H. Chen, and P.-A. Heng. Semantic-aware generative adversarial nets for unsupervised domain adaptation in chest x-ray segmentation. *arXiv preprint arXiv:1806.00600*, 2018.
- [20] X. Chen, Y. Duan, R. Houthoofd, J. Schulman, I. Sutskever, and P. Abbeel. Infogan: Interpretable representation learning by information maximizing generative adversarial nets. In *Advances in Neural Information Processing Systems*, pages 2172–2180, 2016.
- [21] X. Chen and E. Konukoglu. Unsupervised detection of lesions in brain mri using constrained adversarial auto-encoders. *arXiv preprint arXiv:1806.04972*, 2018.
- [22] Y. Chen, F. Shi, A. G. Christodoulou, Z. Zhou, Y. Xie, and D. Li. Efficient and accurate mri super-resolution using a generative adversarial network and 3d multi-level densely connected network. *arXiv preprint arXiv:1803.01417*, 2018.
- [23] H. Choi and D. S. Lee. Generation of structural mr images from amyloid pet: Application to mr-less quantification. *Journal of nuclear medicine: official publication, Society of Nuclear Medicine*, 2017.
- [24] M. J. Chuquicuma, S. Hussein, J. Burt, and U. Bagci. How to fool radiologists with generative adversarial networks? a visual turing test for lung cancer diagnosis.

- arXiv preprint arXiv:1710.09762*, 2017.
- [25] P. Costa, A. Galdran, M. I. Meyer, M. D. Abràmoff, M. Niemeijer, A. M. Mendonça, and A. Campilho. Towards adversarial retinal image synthesis. *arXiv preprint arXiv:1701.08974*, 2017.
 - [26] P. Costa, A. Galdran, M. I. Meyer, M. Niemeijer, M. Abràmoff, A. M. Mendonça, and A. Campilho. End-to-end adversarial retinal image synthesis. *IEEE Transactions on Medical Imaging*, 2017.
 - [27] A. Creswell, T. White, V. Dumoulin, K. Arulkumaran, B. Sengupta, and A. A. Bharath. Generative adversarial networks: An overview. *IEEE Signal Processing Magazine*, 35(1):53–65, 2018.
 - [28] B. Dai, D. Lin, R. Urtasun, and S. Fidler. Towards diverse and natural image descriptions via a conditional gan. *arXiv preprint arXiv:1703.06029*, 2017.
 - [29] W. Dai, J. Doyle, X. Liang, H. Zhang, N. Dong, Y. Li, and E. P. Xing. Scan: Structure correcting adversarial network for chest x-rays organ segmentation. *arXiv preprint arXiv:1703.08770*, 2017.
 - [30] S. U. H. Dar, M. Yurt, L. Karacan, A. Erdem, E. Erdem, and T. Çukur. Image synthesis in multi-contrast mri with conditional generative adversarial networks. *arXiv preprint arXiv:1802.01221*, 2018.
 - [31] S. U. H. Dar, M. Yurt, M. Shahdloo, M. E. Ildiz, and T. Çukur. Synergistic reconstruction and synthesis via generative adversarial networks for accelerated multi-contrast mri. *arXiv preprint arXiv:1805.10704*, 2018.
 - [32] E. L. Denton, S. Chintala, R. Fergus, et al. Deep generative image models using a laplacian pyramid of adversarial networks. In *Advances in neural information processing systems*, pages 1486–1494, 2015.
 - [33] J. Donahue, P. Krähenbühl, and T. Darrell. Adversarial feature learning. *arXiv preprint arXiv:1605.09782*, 2016.
 - [34] Q. Dou, C. Ouyang, C. Chen, H. Chen, and P.-A. Heng. Unsupervised cross-modality domain adaptation of convnets for biomedical image segmentations with adversarial loss. *arXiv preprint arXiv:1804.10916*, 2018.
 - [35] V. Dumoulin, I. Belghazi, B. Poole, A. Lamb, M. Arjovsky, O. Mastropietro, and A. Courville. Adversarially learned inference. *arXiv preprint arXiv:1606.00704*, 2016.
 - [36] H. Emami, M. Dong, S. P. Nejad-Davarani, and C. Glide-Hurst. Generating synthetic ct s from magnetic resonance images using generative adversarial networks. *Medical physics*, 2018.
 - [37] A. Esteva, B. Kuprel, R. A. Novoa, J. Ko, S. M. Swetter, H. M. Blau, and S. Thrun. Dermatologist-level classification of skin cancer with deep neural networks. *Nature*, 542(7639):115, 2017.
 - [38] W. Fedus, I. Goodfellow, and A. M. Dai. Maskgan: Better text generation via filling in the _ . *arXiv preprint arXiv:1801.07736*, 2018.
 - [39] M. Fischer, H. Yang, and C. Meinel. A conditional adversarial network for semantic segmentation of brain tumor. In *Brainlesion: Glioma, Multiple Sclerosis, Stroke and Traumatic Brain Injuries: Third International Workshop, BrainLes 2017, Held in Conjunction with MICCAI 2017, Quebec City, QC, Canada, September 14, 2017, Revised Selected Papers*, volume 10670, page 241. Springer, 2018.
 - [40] C. I. for Health Information. Wait times for priority procedures in canada, 2017.
 - [41] M. Frid-Adar, I. Diamant, E. Klang, M. Amitai, J. Goldberger, and H. Greenspan. Gan-based synthetic medical image augmentation for increased cnn performance in liver lesion classification. *arXiv preprint arXiv:1803.01229*, 2018.
 - [42] K. Fukushima and S. Miyake. Neocognitron: A self-organizing neural network model for a mechanism of visual pattern recognition. In *Competition and cooperation in neural nets*, pages 267–285. Springer, 1982.
 - [43] E. W. Gal Yaniv, Anna Kuperberg. Deep learning algorithm for optimizing critical findings report turnaround time. In *SIIM*, 2018.
 - [44] F. Galbusera, F. Niemeyer, M. Seyfried, T. Bassani, G. Casaroli, A. Kienle, and H.-J. Wilke. Exploring the potential of generative adversarial networks for synthesizing radiological images of the spine to be used in in silico trials. *Frontiers in Bioengineering and Biotechnology*, 6:53, 2018.
 - [45] I. Goodfellow, J. Pouget-Abadie, M. Mirza, B. Xu, D. Warde-Farley, S. Ozair, A. Courville, and Y. Bengio. Generative adversarial nets. In *Advances in neural information processing systems*, pages 2672–2680, 2014.
 - [46] J. T. Guibas, T. S. Virdi, and P. S. Li. Synthetic medical images from dual generative adversarial networks. *arXiv preprint arXiv:1709.01872*, 2017.
 - [47] I. Gulrajani, F. Ahmed, M. Arjovsky, V. Dumoulin, and A. Courville. Improved training of wasserstein gans. *arXiv preprint arXiv:1704.00028*, 2017.
 - [48] V. Gulshan, L. Peng, M. Coram, M. C. Stumpe, D. Wu, A. Narayanaswamy, S. Venugopalan, K. Widner, T. Madams, J. Cuadros, et al. Development and validation of a deep learning algorithm for detection of diabetic retinopathy in retinal fundus photographs. *Jama*, 316(22):2402–2410, 2016.
 - [49] C. Han, H. Hayashi, L. Rundo, R. Araki, W. Shimoda, S. Muramatsu, Y. Furukawa, G. Mauri, and H. Nakayama. Gan-based synthetic brain mr image generation. In *Biomedical Imaging (ISBI 2018), 2018 IEEE 15th International Symposium on*, pages 734–738. IEEE, 2018.
 - [50] M. Heusel, H. Ramsauer, T. Unterthiner, B. Nessler, G. Klambauer, and S. Hochreiter. Gans trained by a two time-scale update rule converge to a nash equilibrium. *arXiv preprint arXiv:1706.08500*, 2017.
 - [51] Y. Hiasa, Y. Otake, M. Takao, T. Matsuoka, K. Takashima, J. L. Prince, N. Sugano, and Y. Sato. Cross-modality image synthesis from unpaired data using cyclegan: Effects of gradient consistency loss and training data size. *arXiv preprint arXiv:1803.06629*, 2018.
 - [52] L. Hou, A. Agarwal, D. Samaras, T. M. Kurc, R. R. Gupta, and J. H. Saltz. Unsupervised histopathology image synthesis. *arXiv preprint arXiv:1712.05021*,

- 2017.
- [53] B. Hu, Y. Tang, E. I. Chang, Y. Fan, M. Lai, Y. Xu, et al. Unsupervised learning for cell-level visual representation in histopathology images with generative adversarial networks. *arXiv preprint arXiv:1711.11317*, 2017.
 - [54] Y. Hu, E. Gibson, L.-L. Lee, W. Xie, D. C. Barratt, T. Vercauteren, and J. A. Noble. Freehand ultrasound image simulation with spatially-conditioned generative adversarial networks. In *Molecular Imaging, Reconstruction and Analysis of Moving Body Organs, and Stroke Imaging and Treatment*, pages 105–115. Springer, 2017.
 - [55] Y. Hu, E. Gibson, T. Vercauteren, H. U. Ahmed, M. Emberton, C. M. Moore, J. A. Noble, and D. C. Barratt. Intraoperative organ motion models with an ensemble of conditional generative adversarial networks. In *International Conference on Medical Image Computing and Computer-Assisted Intervention*, pages 368–376. Springer, 2017.
 - [56] H. Huang, P. S. Yu, and C. Wang. An introduction to image synthesis with generative adversarial nets. *arXiv preprint arXiv:1803.04469*, 2018.
 - [57] X. Huang, Y. Li, O. Poursaeed, J. E. Hopcroft, and S. J. Belongie. Stacked generative adversarial networks. In *CVPR*, volume 2, page 3, 2017.
 - [58] Y. Huo, Z. Xu, S. Bao, A. Assad, R. G. Abramson, and B. A. Landman. Adversarial synthesis learning enables segmentation without target modality ground truth. *arXiv preprint arXiv:1712.07695*, 2017.
 - [59] Y. Huo, Z. Xu, S. Bao, C. Bermudez, A. J. Plassard, J. Liu, Y. Yao, A. Assad, R. G. Abramson, and B. A. Landman. Splenomegaly segmentation using global convolutional kernels and conditional generative adversarial networks. In *Medical Imaging 2018: Image Processing*, volume 10574, page 1057409. International Society for Optics and Photonics, 2018.
 - [60] S. Ioffe and C. Szegedy. Batch normalization: Accelerating deep network training by reducing internal covariate shift. *arXiv preprint arXiv:1502.03167*, 2015.
 - [61] P. Isola, J.-Y. Zhu, T. Zhou, and A. A. Efros. Image-to-image translation with conditional adversarial networks. *arXiv preprint arXiv:1611.07004*, 2016.
 - [62] S. Izadi, Z. Mirikharaji, J. Kawahara, and G. Hamarneh. Generative adversarial networks to segment skin lesions. In *Biomedical Imaging (ISBI 2018), 2018 IEEE 15th International Symposium on*, pages 881–884. IEEE, 2018.
 - [63] M. Jaderberg, K. Simonyan, A. Zisserman, et al. Spatial transformer networks. In *Advances in neural information processing systems*, pages 2017–2025, 2015.
 - [64] J. M. F. A.-a. T. V. A. R. M. O. Jae Ho Sohn, Hari Trivedi. Development and validation of machine learning based natural language classifiers to automatically assign mri abdomen/pelvis protocols from free-text clinical indications. In *SIIM*, 2017.
 - [65] C.-B. Jin, W. Jung, S. Joo, E. Park, A. Y. Saem, I. H. Han, J. I. Lee, and X. Cui. Deep ct to mr synthesis using paired and unpaired data. *arXiv preprint arXiv:1805.10790*, 2018.
 - [66] B. Jing, P. Xie, and E. Xing. On the automatic generation of medical imaging reports. *arXiv preprint arXiv:1711.08195*, 2017.
 - [67] K. Kamnitsas, C. Baumgartner, C. Ledig, V. Newcombe, J. Simpson, A. Kane, D. Menon, A. Nori, A. Criminisi, D. Rueckert, et al. Unsupervised domain adaptation in brain lesion segmentation with adversarial networks. In *International Conference on Information Processing in Medical Imaging*, pages 597–609. Springer, 2017.
 - [68] E. Kang, H. J. Koo, D. H. Yang, J. B. Seo, and J. C. Ye. Cycle consistent adversarial denoising network for multiphase coronary ct angiography. *arXiv preprint arXiv:1806.09748*, 2018.
 - [69] T. Karras, T. Aila, S. Laine, and J. Lehtinen. Progressive growing of gans for improved quality, stability, and variation. *arXiv preprint arXiv:1710.10196*, 2017.
 - [70] K. H. Kim, W.-J. Do, and S.-H. Park. Improving resolution of mr images with an adversarial network incorporating images with different contrast. *Medical physics*, 2018.
 - [71] T. Kim, M. Cha, H. Kim, J. K. Lee, and J. Kim. Learning to discover cross-domain relations with generative adversarial networks. *arXiv preprint arXiv:1703.05192*, 2017.
 - [72] N. Kodali, J. Abernethy, J. Hays, and Z. Kira. On convergence and stability of gans. *arXiv preprint arXiv:1705.07215*, 2017.
 - [73] S. Kohl, D. Bonekamp, H.-P. Schlemmer, K. Yaqubi, M. Hohenfellner, B. Hadaschik, J.-P. Radtke, and K. Maier-Hein. Adversarial networks for the detection of aggressive prostate cancer. *arXiv preprint arXiv:1702.08014*, 2017.
 - [74] T. Köhler, A. Budai, M. F. Kraus, J. Odstrčilík, G. Michelson, and J. Hornegger. Automatic no-reference quality assessment for retinal fundus images using vessel segmentation. In *Computer-Based Medical Systems (CBMS), 2013 IEEE 26th International Symposium on*, pages 95–100. IEEE, 2013.
 - [75] D. Korkinof, T. Rijken, M. O’Neill, J. Yearsley, H. Harvey, and B. Glocker. High-resolution mammogram synthesis using progressive generative adversarial networks. *arXiv preprint arXiv:1807.03401*, 2018.
 - [76] A. Krizhevsky, I. Sutskever, and G. E. Hinton. Imagenet classification with deep convolutional neural networks. In *Advances in neural information processing systems*, pages 1097–1105, 2012.
 - [77] K. Kurach, M. Lucic, X. Zhai, M. Michalski, and S. Gelly. The gan landscape: Losses, architectures, regularization, and normalization. 2018.
 - [78] A. Lahiri, K. Ayush, P. K. Biswas, and P. Mitra. Generative adversarial learning for reducing manual annotation in semantic segmentation on large scale microscopy images: Automated vessel segmentation in retinal fundus image as test case. In *Conference on Computer Vision and Pattern Recognition Workshops*, pages 42–48, 2017.
 - [79] A. B. L. Larsen, S. K. Sørderby, H. Larochelle, and O. Winther. Autoencoding beyond pixels us-

- ing a learned similarity metric. *arXiv preprint arXiv:1512.09300*, 2015.
- [80] G. Larsson, M. Maire, and G. Shakhnarovich. Colorization as a proxy task for visual understanding. In *CVPR*, volume 2, page 7, 2017.
- [81] C. Ledig, L. Theis, F. Huszár, J. Caballero, A. Cunningham, A. Acosta, A. Aitken, A. Tejani, J. Totz, Z. Wang, et al. Photo-realistic single image super-resolution using a generative adversarial network. *arXiv preprint*, 2017.
- [82] Y. Li and L. Shen. cc-gan: A robust transfer-learning framework for hep-2 specimen image segmentation. *IEEE Access*, 6:14048–14058, 2018.
- [83] Z. Li, Y. Wang, and J. Yu. Brain tumor segmentation using an adversarial network. In *International MICCAI Brainlesion Workshop*, pages 123–132. Springer, 2017.
- [84] Z. Li, Y. Wang, and J. Yu. Reconstruction of thin-slice medical images using generative adversarial network. In *International Workshop on Machine Learning in Medical Imaging*, pages 325–333. Springer, 2017.
- [85] G. Litjens, T. Kooi, B. E. Bejnordi, A. A. A. Setio, F. Ciompi, M. Ghafoorian, J. A. van der Laak, B. van Ginneken, and C. I. Sánchez. A survey on deep learning in medical image analysis. *arXiv preprint arXiv:1702.05747*, 2017.
- [86] M.-Y. Liu, T. Breuel, and J. Kautz. Unsupervised image-to-image translation networks. In *Advances in Neural Information Processing Systems*, pages 700–708, 2017.
- [87] P. Liu, X. Qiu, and X. Huang. Adversarial multi-task learning for text classification. *arXiv preprint arXiv:1704.05742*, 2017.
- [88] J. Long, E. Shelhamer, and T. Darrell. Fully convolutional networks for semantic segmentation. In *Proceedings of the IEEE conference on computer vision and pattern recognition*, pages 3431–3440, 2015.
- [89] A. L. Maas, A. Y. Hannun, and A. Y. Ng. Rectifier nonlinearities improve neural network acoustic models. In *Proc. icml*, volume 30, page 3, 2013.
- [90] A. Madani, M. Moradi, A. Karargyris, and T. Syeda-Mahmood. Chest x-ray generation and data augmentation for cardiovascular abnormality classification. In *Medical Imaging 2018: Image Processing*, volume 10574, page 105741M. International Society for Optics and Photonics, 2018.
- [91] A. Madani, M. Moradi, A. Karargyris, and T. Syeda-Mahmood. Semi-supervised learning with generative adversarial networks for chest x-ray classification with ability of data domain adaptation. In *Biomedical Imaging (ISBI 2018), 2018 IEEE 15th International Symposium on*, pages 1038–1042. IEEE, 2018.
- [92] D. Mahapatra. Retinal vasculature segmentation using local saliency maps and generative adversarial networks for image super resolution. *arXiv preprint arXiv:1710.04783*, 2017.
- [93] D. Mahapatra, B. Antony, S. Sedai, and R. Garnavi. Deformable medical image registration using generative adversarial networks. In *Biomedical Imaging (ISBI 2018), 2018 IEEE 15th International Symposium on*, pages 1449–1453. IEEE, 2018.
- [94] F. Mahmood, R. Chen, and N. J. Durr. Unsupervised reverse domain adaption for synthetic medical images via adversarial training. *arXiv preprint arXiv:1711.06606*, 2017.
- [95] X. Mao, Q. Li, H. Xie, R. Y. Lau, and Z. Wang. Least squares generative adversarial networks. *arXiv preprint arXiv:1611.04076*, 2016.
- [96] M. Mardani, E. Gong, J. Y. Cheng, S. Vasanaawala, G. Zaharchuk, M. Alley, N. Thakur, S. Han, W. Dally, J. M. Pauly, et al. Deep generative adversarial networks for compressed sensing automates mri. *arXiv preprint arXiv:1706.00051*, 2017.
- [97] I. Melnyk, T. Sercu, P. L. Dognin, J. Ross, and Y. Mroueh. Improved image captioning with adversarial semantic alignment. *arXiv preprint arXiv:1805.00063*, 2018.
- [98] F. Milletari, N. Navab, and S.-A. Ahmadi. V-net: Fully convolutional neural networks for volumetric medical image segmentation. In *3D Vision (3DV), 2016 Fourth International Conference on*, pages 565–571. IEEE, 2016.
- [99] M. Mirza and S. Osindero. Conditional generative adversarial nets. *arXiv preprint arXiv:1411.1784*, 2014.
- [100] T. Miyato, T. Kataoka, M. Koyama, and Y. Yoshida. Spectral normalization for generative adversarial networks. *arXiv preprint arXiv:1802.05957*, 2018.
- [101] T. Miyato and M. Koyama. cgans with projection discriminator. *arXiv preprint arXiv:1802.05637*, 2018.
- [102] P. Moeskops, M. Veta, M. W. Lafarge, K. A. Eppenhof, and J. P. Pluim. Adversarial training and dilated convolutions for brain mri segmentation. In *Deep Learning in Medical Image Analysis and Multimodal Learning for Clinical Decision Support*, pages 56–64. Springer, 2017.
- [103] T. C. Mok and A. C. Chung. Learning data augmentation for brain tumor segmentation with coarse-to-fine generative adversarial networks. *arXiv preprint arXiv:1805.11291*, 2018.
- [104] T. Neff, C. Payer, D. Štern, and M. Urschler. Generative adversarial network based synthesis for supervised medical image segmentation. 2017.
- [105] D. Nie, R. Trullo, J. Lian, C. Petitjean, S. Ruan, Q. Wang, and D. Shen. Medical image synthesis with context-aware generative adversarial networks. In *International Conference on Medical Image Computing and Computer-Assisted Intervention*, pages 417–425. Springer, 2017.
- [106] D. Nie, R. Trullo, J. Lian, L. Wang, C. Petitjean, S. Ruan, Q. Wang, and D. Shen. Medical image synthesis with deep convolutional adversarial networks. *IEEE Transactions on Biomedical Engineering*, 2018.
- [107] M. Niemeijer, M. D. Abramoff, and B. van Ginneken. Image structure clustering for image quality verification of color retina images in diabetic retinopathy screening. *Medical image analysis*, 10(6):888–898, 2006.
- [108] S. Nowozin, B. Cseke, and R. Tomioka. f-gan: Training generative neural samplers using variational divergence minimization. In *Advances in Neural Information Processing Systems*, pages 271–279, 2016.
- [109] A. Odena, C. Olah, and J. Shlens. Conditional image

- synthesis with auxiliary classifier gans. *arXiv preprint arXiv:1610.09585*, 2016.
- [110] D. S. of the Clinical Practice Committee et al. Informed consent for medical photographs. *Genetics in Medicine*, 2(6):353, 2000.
- [111] S. Olut, Y. H. Sahin, U. Demir, and G. Unal. Generative adversarial training for mra image synthesis using multi-contrast mri. *arXiv preprint arXiv:1804.04366*, 2018.
- [112] N. Pandhe, B. Rada, and S. Quinn. Generative spatiotemporal modeling of neutrophil behavior. In *Biomedical Imaging (ISBI 2018), 2018 IEEE 15th International Symposium on*, pages 969–972. IEEE, 2018.
- [113] D. Pathak, P. Krahenbuhl, J. Donahue, T. Darrell, and A. A. Efros. Context encoders: Feature learning by inpainting. In *Proceedings of the IEEE Conference on Computer Vision and Pattern Recognition*, pages 2536–2544, 2016.
- [114] C. Peng, X. Zhang, G. Yu, G. Luo, and J. Sun. Large kernel matters—improve semantic segmentation by global convolutional network. In *Computer Vision and Pattern Recognition (CVPR), 2017 IEEE Conference on*, pages 1743–1751. IEEE, 2017.
- [115] T. M. Quan, T. Nguyen-Duc, and W.-K. Jeong. Compressed sensing mri reconstruction with cyclic loss in generative adversarial networks. *arXiv preprint arXiv:1709.00753*, 2017.
- [116] T. M. Quan, T. Nguyen-Duc, and W.-K. Jeong. Compressed sensing mri reconstruction using a generative adversarial network with a cyclic loss. *IEEE transactions on medical imaging*, 37(6):1488–1497, 2018.
- [117] A. Radford, L. Metz, and S. Chintala. Unsupervised representation learning with deep convolutional generative adversarial networks. *arXiv preprint arXiv:1511.06434*, 2015.
- [118] D. Ravi, A. B. Szczotka, D. I. Shakir, S. P. Pereira, and T. Vercauteren. Adversarial training with cycle consistency for unsupervised super-resolution in endomicroscopy. 2018.
- [119] S. Reed, Z. Akata, X. Yan, L. Logeswaran, B. Schiele, and H. Lee. Generative adversarial text to image synthesis. In *Proceedings of The 33rd International Conference on Machine Learning*, volume 3, 2016.
- [120] S. E. Reed, Z. Akata, S. Mohan, S. Tenka, B. Schiele, and H. Lee. Learning what and where to draw. In *Advances in Neural Information Processing Systems*, pages 217–225, 2016.
- [121] M. Rezaei, K. Harmuth, W. Gierke, T. Kellermeier, M. Fischer, H. Yang, and C. Meinel. Conditional adversarial network for semantic segmentation of brain tumor. *arXiv preprint arXiv:1708.05227*, 2017.
- [122] M. Rezaei, H. Yang, and C. Meinel. Whole heart and great vessel segmentation with context-aware of generative adversarial networks. In *Bildverarbeitung für die Medizin 2018*, pages 353–358. Springer, 2018.
- [123] O. Ronneberger, P. Fischer, and T. Brox. U-net: Convolutional networks for biomedical image segmentation. In *International Conference on Medical image computing and computer-assisted intervention*, pages 234–241. Springer, 2015.
- [124] T. Ross, D. Zimmerer, A. Vemuri, F. Isensee, M. Wiesenfarth, S. Bodenstedt, F. Both, P. Kessler, M. Wagner, B. Müller, et al. Exploiting the potential of unlabeled endoscopic video data with self-supervised learning. *International journal of computer assisted radiology and surgery*, pages 1–9, 2018.
- [125] H. Salehinejad, S. Valaee, T. Dowdell, E. Colak, and J. Barfett. Generalization of deep neural networks for chest pathology classification in x-rays using generative adversarial networks. *arXiv preprint arXiv:1712.01636*, 2017.
- [126] T. Salimans, I. Goodfellow, W. Zaremba, V. Cheung, A. Radford, and X. Chen. Improved techniques for training gans. In *Advances in Neural Information Processing Systems*, pages 2226–2234, 2016.
- [127] I. Sanchez and V. Vilaplana. Brain mri super-resolution using 3d generative adversarial networks. 2018.
- [128] P. Sangkloy, J. Lu, C. Fang, F. Yu, and J. Hays. Scribbler: Controlling deep image synthesis with sketch and color. *arXiv preprint arXiv:1612.00835*, 2016.
- [129] T. Schlegl, P. Seeböck, S. M. Waldstein, U. Schmidt-Erfurth, and G. Langs. Unsupervised anomaly detection with generative adversarial networks to guide marker discovery. In *International Conference on Information Processing in Medical Imaging*, pages 146–157. Springer, 2017.
- [130] C. Senaras, M. K. K. Niazi, B. Sahiner, M. P. Pennell, G. Tozbikian, G. Lozanski, and M. N. Gurcan. Optimized generation of high-resolution phantom images using cgan: Application to quantification of ki67 breast cancer images. *PloS one*, 13(5):e0196846, 2018.
- [131] M. T. Shaban, C. Baur, N. Navab, and S. Albarqouni. Staingan: Stain style transfer for digital histological images. *arXiv preprint arXiv:1804.01601*, 2018.
- [132] S. M. Shankaranarayana, K. Ram, K. Mitra, and M. Sivaprakasam. Joint optic disc and cup segmentation using fully convolutional and adversarial networks. In *Fetal, Infant and Ophthalmic Medical Image Analysis*, pages 168–176. Springer, 2017.
- [133] H. R. Sheikh and A. C. Bovik. Image information and visual quality. In *Acoustics, Speech, and Signal Processing, 2004. Proceedings.(ICASSP'04). IEEE International Conference on*, volume 3, pages iii–709. IEEE, 2004.
- [134] R. Shetty, M. Rohrbach, L. A. Hendricks, M. Fritz, and B. Schiele. Speaking the same language: Matching machine to human captions by adversarial training. In *Proceedings of the IEEE International Conference on Computer Vision (ICCV)*, 2017.
- [135] O. Shitrit and T. R. Raviv. Accelerated magnetic resonance imaging by adversarial neural network. In *Deep Learning in Medical Image Analysis and Multimodal Learning for Clinical Decision Support*, pages 30–38. Springer, 2017.
- [136] P. Y. Simard, D. Steinkraus, and J. C. Platt. Best practices for convolutional neural networks applied to visual document analysis. In *null*, page 958. IEEE, 2003.

- [137] K. Simonyan and A. Zisserman. Very deep convolutional networks for large-scale image recognition. *arXiv preprint arXiv:1409.1556*, 2014.
- [138] V. K. Singh, H. Rashwan, F. Akram, N. Pandey, M. Sarker, M. Kamal, A. Saleh, S. Abdulwahab, N. Maarroof, S. Romani, et al. Retinal optic disc segmentation using conditional generative adversarial network. *arXiv preprint arXiv:1806.03905*, 2018.
- [139] J. Son, S. J. Park, and K.-H. Jung. Retinal vessel segmentation in fundoscopic images with generative adversarial networks. *arXiv preprint arXiv:1706.09318*, 2017.
- [140] J. T. Springenberg. Unsupervised and semi-supervised learning with categorical generative adversarial networks. *arXiv preprint arXiv:1511.06390*, 2015.
- [141] C. Tanner, F. Ozdemir, R. Profanter, V. Vishnevsky, E. Konukoglu, and O. Goksel. Generative adversarial networks for mr-ct deformable image registration. *arXiv preprint arXiv:1807.07349*, 2018.
- [142] A. Udrea and G. D. Mitra. Generative adversarial neural networks for pigmented and non-pigmented skin lesions detection in clinical images. In *Control Systems and Computer Science (CSCS), 2017 21st International Conference on*, pages 364–368. IEEE, 2017.
- [143] D. Wang, C. Gu, K. Wu, and X. Guan. Adversarial neural networks for basal membrane segmentation of microinvasive cervix carcinoma in histopathology images. In *Machine Learning and Cybernetics (ICMLC), 2017 International Conference on*, volume 2, pages 385–389. IEEE, 2017.
- [144] T.-C. Wang, M.-Y. Liu, J.-Y. Zhu, A. Tao, J. Kautz, and B. Catanzaro. High-resolution image synthesis and semantic manipulation with conditional gans. *arXiv preprint arXiv:1711.11585*, 2017.
- [145] Y. Wang, B. Yu, L. Wang, C. Zu, D. S. Lalush, W. Lin, X. Wu, J. Zhou, D. Shen, and L. Zhou. 3d conditional generative adversarial networks for high-quality pet image estimation at low dose. *NeuroImage*, 174:550–562, 2018.
- [146] Z. Wang and A. C. Bovik. A universal image quality index. *IEEE signal processing letters*, 9(3):81–84, 2002.
- [147] Z. Wang, A. C. Bovik, H. R. Sheikh, and E. P. Simoncelli. Image quality assessment: from error visibility to structural similarity. *IEEE transactions on image processing*, 13(4):600–612, 2004.
- [148] W. Wei, E. Poirion, B. Bodini, S. Durrleman, N. Ayache, B. Stankoff, and O. Colliot. Learning myelin content in multiple sclerosis from multimodal mri through adversarial training. *arXiv preprint arXiv:1804.08039*, 2018.
- [149] P. Welandar, S. Karlsson, and A. Eklund. Generative adversarial networks for image-to-image translation on multi-contrast mr images—a comparison of cyclegan and unit. *arXiv preprint arXiv:1806.07777*, 2018.
- [150] J. M. Wolterink, A. M. Dinkla, M. H. Savenije, P. R. Seevinck, C. A. van den Berg, and I. Išgum. Deep mr to ct synthesis using unpaired data. In *International Workshop on Simulation and Synthesis in Medical Imaging*, pages 14–23. Springer, 2017.
- [151] J. M. Wolterink, T. Leiner, and I. Išgum. Blood vessel geometry synthesis using generative adversarial networks. *arXiv preprint arXiv:1804.04381*, 2018.
- [152] J. M. Wolterink, T. Leiner, M. A. Viergever, and I. Išgum. Generative adversarial networks for noise reduction in low-dose ct. *IEEE Transactions on Medical Imaging*, 2017.
- [153] T. Xu, P. Zhang, Q. Huang, H. Zhang, Z. Gan, X. Huang, and X. He. AttnGAN: Fine-grained text to image generation with attentional generative adversarial networks. *arXiv preprint*, 2017.
- [154] Y. Xue, T. Xu, H. Zhang, R. Long, and X. Huang. Segan: Adversarial network with multi-scale l_1 loss for medical image segmentation. *arXiv preprint arXiv:1706.01805*, 2017.
- [155] A. Yadav, S. Shah, Z. Xu, D. Jacobs, and T. Goldstein. Stabilizing adversarial nets with prediction methods. 2018.
- [156] P. Yan, S. Xu, A. R. Rastinehad, and B. J. Wood. Adversarial image registration with application for mr and trus image fusion. *arXiv preprint arXiv:1804.11024*, 2018.
- [157] D. Yang, D. Xu, S. K. Zhou, B. Georgescu, M. Chen, S. Grbic, D. Metaxas, and D. Comaniciu. Automatic liver segmentation using an adversarial image-to-image network. In *International Conference on Medical Image Computing and Computer-Assisted Intervention*, pages 507–515. Springer, 2017.
- [158] Q. Yang, N. Li, Z. Zhao, X. Fan, E. I. Chang, Y. Xu, et al. Mri image-to-image translation for cross-modality image registration and segmentation. *arXiv preprint arXiv:1801.06940*, 2018.
- [159] Q. Yang, P. Yan, Y. Zhang, H. Yu, Y. Shi, X. Mou, M. K. Kalra, and G. Wang. Low dose ct image denoising using a generative adversarial network with wasserstein distance and perceptual loss. *arXiv preprint arXiv:1708.00961*, 2017.
- [160] X. Yi and P. Babyn. Sharpness-aware low-dose ct denoising using conditional generative adversarial network. *Journal of digital imaging*, pages 1–15, 2018.
- [161] X. Yi, E. Walia, and P. Babyn. Unsupervised and semi-supervised learning with categorical generative adversarial networks assisted by wasserstein distance for dermoscopy image classification. *arXiv preprint arXiv:1804.03700*, 2018.
- [162] C. You, Q. Yang, H. Shan, L. Gjestebj, L. Guang, S. Ju, Z. Zhang, Z. Zhao, Y. Zhang, W. Cong, et al. Structure-sensitive multi-scale deep neural network for low-dose ct denoising. *arXiv preprint arXiv:1805.00587*, 2018.
- [163] B. Yu, L. Zhou, L. Wang, J. Frapp, and P. Bourgeat. 3d cgan based cross-modality mr image synthesis for brain tumor segmentation. In *Biomedical Imaging (ISBI 2018), 2018 IEEE 15th International Symposium on*, pages 626–630. IEEE, 2018.
- [164] S. Yu, H. Dong, G. Yang, G. Slabaugh, P. L. Dragotti, X. Ye, F. Liu, S. Arridge, J. Keegan, D. Firmin, et al. Deep de-aliasing for fast compressive sensing mri. *arXiv preprint arXiv:1705.07137*, 2017.
- [165] F. G. Zanjani, S. Zinger, B. E. Bejnordi, J. A. van der Laak, and P. H. de With. Stain normalization of

- histopathology images using generative adversarial networks. In *Biomedical Imaging (ISBI 2018)*, 2018 *IEEE 15th International Symposium on*, pages 573–577. IEEE, 2018.
- [166] F. G. Zanjani, S. Zinger, B. E. Bejnordi, J. A. van der Laak, et al. Histopathology stain-color normalization using generative neural networks. 2018.
 - [167] H. Zhang, T. Xu, H. Li, S. Zhang, X. Huang, X. Wang, and D. Metaxas. Stackgan: Text to photo-realistic image synthesis with stacked generative adversarial networks. In *IEEE Int. Conf. Comput. Vision (ICCV)*, pages 5907–5915, 2017.
 - [168] L. Zhang, A. Gooya, and A. F. Frangi. Semi-supervised assessment of incomplete lv coverage in cardiac mri using generative adversarial nets. In *International Workshop on Simulation and Synthesis in Medical Imaging*, pages 61–68. Springer, 2017.
 - [169] R. Zhang, P. Isola, A. A. Efros, E. Shechtman, and O. Wang. The unreasonable effectiveness of deep features as a perceptual metric. *arXiv preprint*, 2018.
 - [170] Y. Zhang, S. Miao, T. Mansi, and R. Liao. Task driven generative modeling for unsupervised domain adaptation: Application to x-ray image segmentation. *arXiv preprint arXiv:1806.07201*, 2018.
 - [171] Y. Zhang, L. Yang, J. Chen, M. Fredericksen, D. P. Hughes, and D. Z. Chen. Deep adversarial networks for biomedical image segmentation utilizing unannotated images. In *International Conference on Medical Image Computing and Computer-Assisted Intervention*, pages 408–416. Springer, 2017.
 - [172] Z. Zhang, L. Yang, and Y. Zheng. Translating and segmenting multimodal medical volumes with cycle-and shape-consistency generative adversarial network. *arXiv preprint arXiv:1802.09655*, 2018.
 - [173] H. Zhao, H. Li, and L. Cheng. Synthesizing filamentary structured images with gans. *arXiv preprint arXiv:1706.02185*, 2017.
 - [174] J. Zhao, M. Mathieu, and Y. LeCun. Energy-based generative adversarial network. *arXiv preprint arXiv:1609.03126*, 2016.
 - [175] J.-Y. Zhu, T. Park, P. Isola, and A. A. Efros. Unpaired image-to-image translation using cycle-consistent adversarial networks. *arXiv preprint arXiv:1703.10593*, 2017.
 - [176] W. Zhu, X. Xiang, T. D. Tran, G. D. Hager, and X. Xie. Adversarial deep structured nets for mass segmentation from mammograms. *arXiv preprint arXiv:1710.09288*, 2017.
 - [177] W. Zhu, X. Xiang, T. D. Tran, and X. Xie. Adversarial deep structural networks for mammographic mass segmentation. *arXiv preprint arXiv:1612.05970*, 2016.